ISSN 1070-3632, Russian Journal of General Chemistry, 2018, Vol. 88, No. 2, pp. 199–207. © Pleiades Publishing, Ltd., 2018.
Original Russian Text © L.O. Nindakova, V.O. Strakhov, S.S. Kolesnikov, 2018, published in Zhurnal Obshchei Khimii, 2018, Vol. 88, No. 2, pp. 219–227.

Hydrogenation of Ketones on Dispersed Chiral-Modified Palladium Nanoparticles

L. O. Nindakova*, V. O. Strakhov, and S. S. Kolesnikov

Irkutsk National Research Technical University, ul. Lermontova 83, Irkutsk, 664074 Russia
**e-mail: nindakova@istu.edu*

Received July 20, 2017

Abstract—Hydrogenation of acetophenone and esters of ketoacids with molecular hydrogen in the presence of the $Pd(acac)_2$–(–)-cinchonidine–H_2 catalytic system has been studied. The dependence of the molar ratio of (–)-cinchonidine/Pd on size and shape of palladium nanoparticles, formed in the system, also on reaction rate and enantioselectivity has been established. The nature of the regularities observed for the $Pd(acac)_2$–(–)-cinchonidine–H_2 catalytic system was discussed.

Keywords: palladium nanoparticles, chiral modification, cinchonidine, hydrogenation

DOI: 10.1134/S1070363218020044

Metal nanoparticles are used in catalysis due to their high chemical reactivity and the ability to catalyze novel reaction pathways that do not occur using conventional catalysts [1]. Their use as catalysts of various chemical processes including reducing of the pollutants emission, raw materials processing, synthesis of basic organic species, and energy production is favorable in view of the possibility of immobilization of metal particles on heterogeneous carriers and their regeneration. One of the most promising strategies of the "green" chemistry targeted at the fine chemistry products preparation is the combination of chiral technology and nanotechnology. However, the range of enantioselective catalytic systems involving metal nanoparticles has remained limited. The most important issues related to this research are methods of synthesis of metal nanoparticles [2–9], their functionalization [10–19], special features of their catalysis application [7, 14–21], and the mechanisms of asymmetric reactions [22–31].

One of the first mentions of metal colloids protected by optically active stabilizers may induce enantioselectivity in catalytic hydrogenation with molecular hydrogen was given in [26]. The chiral assemblies at the surface of metal nanoparticles can be constructed via adsorption of optically active pure organic materials (ligands). Since they can stabilize and/or modify the metal nanoparticles, chiral ligands are often referred to as stabilizers and modifiers.

3*S*,8*S*,9*R*-(–)-Cinchonidine is a natural alkaloid containing three chiral centers, important reactant and modifier of catalytic systems based on transition metals [18–23]. It has been found that in the case of Pt/Al_2O_3 (–)-cinchonidine generates chiral regions upon chemisorption on achiral metal surface, and discrimination of enantioface sides of the substrate occurs via the 1 : 1 interaction between the adsorbed substrate and the modifier [18, 20–22]. Analysis of the available reports has revealed that the reaction of enantioselective hydrogenation of prochiral C=O bond in ketones and esters of methyl pyruvate in the presence of immobilized platinum catalysts is well studied, but palladium systems have been rarely used for this purpose. The values of enantiomer excess (*ee*) for reactions catalyzed by metal colloids are low, except for Pt [26]. For example, poly(*N*-vinylpyrrolidone)-stabilized Rh_{coll} has given *ee* 42% for ethyl lactate and (similarly to Pt_{coll}) the increase in the rate with the increased (–)-cinchonidine concentration [32]. In the case of Pd_{coll} stabilized by polymeric surfactant KD1, *ee* 29% has been obtained for ethyl lactate [33], and for poly(*N*-vinylpyrrolidone)-stabilized Ir_{coll} and methyl lactate *ee* has been 34% [34].

This work aimed to study the enantioselective hydrogenation of ketones on Pd nanoparticles applied in the form of colloidal suspension prepared in the $Pd(acac)_2$–(–)-cinchonidine–H_2 system.

Enantioselective hydrogenation of acetophenone. Colloidal systems tested as catalysts for hydrogenation

Scheme 1.

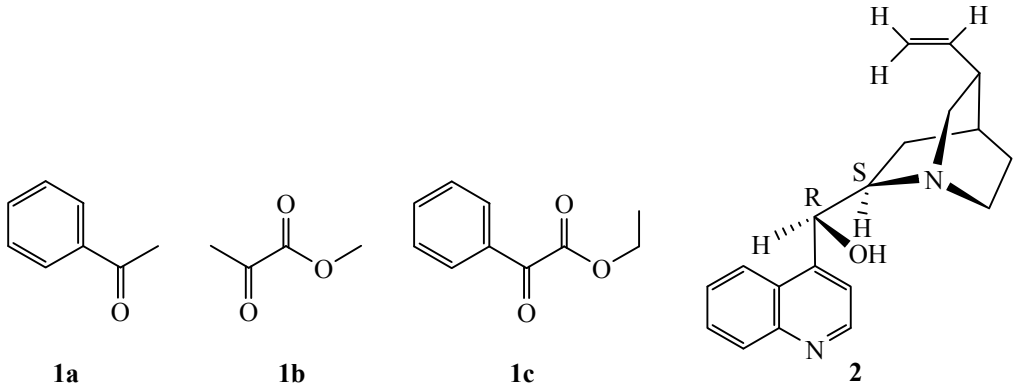

1a **1b** **1c** **2**

of acetophenone **1a**, methyl pyruvate **1b**, and ethyl benzoylformate **1c** under similar conditions were formed via reduction of Pd^{2+} compounds with molecular hydrogen in methanol solution in the presence of chiral chinchona alkaloid (3*S*,8*S*,9*R*)-(–)-cinchonidine **2** (Scheme 1).

(–)-Cinchonidine molecule contains three basic elements: quinoline aromatic moiety, quinuclidine ring with tertiary nitrogen atom, and bridging carbinol group connecting the first two fragments. A key element responsible for the use of this compound as chirality inductor is likely the nucleophilic quinuclidine nitrogen atom in chiral surrounding created by neighbor carbon atoms with *R* and *S* configuration.

Conditions of the experiment [nature of solvent and the (–)-2/Pd ratio] were varied to elucidate their effect on the process rate and stereoselectivity of acetophenone hydrogenation. The only product was formed, 1-phenylethanol.

Typical kinetic curves were S-shaped, with the induction period evidencing the initial formation of the active form of the catalyst. Moreover, the reaction rate was increased after several hours (sometimes after a day), probably due to the formation of palladium nanoparticles of optimal size (Fig. 1). The typical experimental results are collected in Table 1.

Scheme 2.

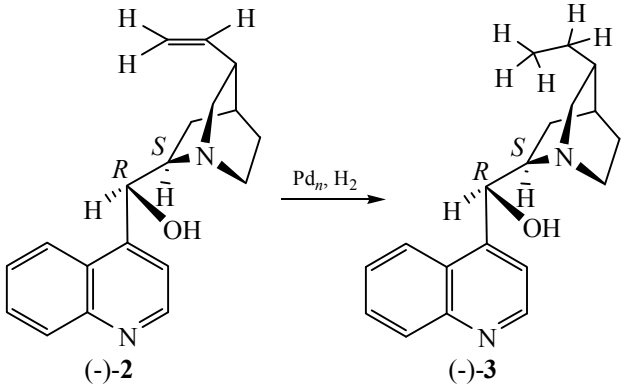

(-)-**2** (-)-**3**

The w_{max}, average particles size, and enantioselectivity of the reaction as functions of the (–)-**2**/Pd molar ratio are given in Fig. 2. The highest process rate (11 mmol L^{-1} h^{-1}) was observed in the absence of any modifier, and the increase in the concentration of (–)-cinchonidine resulted in the deceleration of the reaction, down to 1.1 mmol L^{-1} h^{-1} at (–)–**2**/Pd = 8 : 1. Over the (–)–**2**/Pd range of 1.5–3 the reaction rate was approximately constant, evidencing the saturation of the system with the modifier at (–)-**2**/Pd above 1 : 1. However, the enantioselectivity of the reaction was nonlinear: at ratios range 0–1 the excess of the *S*-enantiomer product grew to 22%, then went down to 4% at ratio 1.5, steadily grew to 27%, and then slightly decreased at the ratio of 8.

In view of the presence of an ethylene substituent at the quinuclidine fragment in the (–)-cinchonidine molecule, we monitored the change in the modifier concentration in the $Pd(acac)_2$–(–)-**2**–H_2 system at the (–)-**2**/Pd molar ratio 4 : 1. In was found that even before the hydrogenation of acetophenone, during the induction period, (–)-cinchonidine was completely converted in (–)-dihydrocinchonidine (–)-**3** (Scheme 2), and evidently stabilization and modification of the formed palladium nanoparticles under the action of compound (–)-**3**.

To elucidate the nature of the catalysis, the solid phase was isolated from the catalytic system using a filter with 200 nm pores size after the constant rate of acetophenone hydrogenation was reached. That procedure did not affect the reaction rate, hence the particles larger than 200 nm were catalytically inactive.

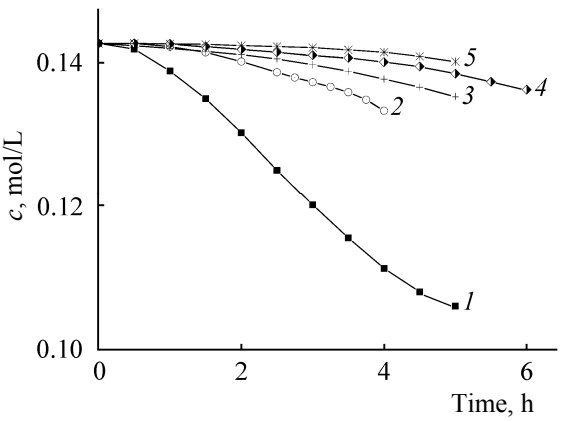

Fig. 1. Kinetic curves of acetophenone hydrogenation in the presence of the $Pd(acac)_2$–(–)-**2**–H_2 system at the (–)-**2** : Pd ratio 0 (*1*), 0.5 (*2*), 4 (*3*), 2 (*4*), 8 (*5*).

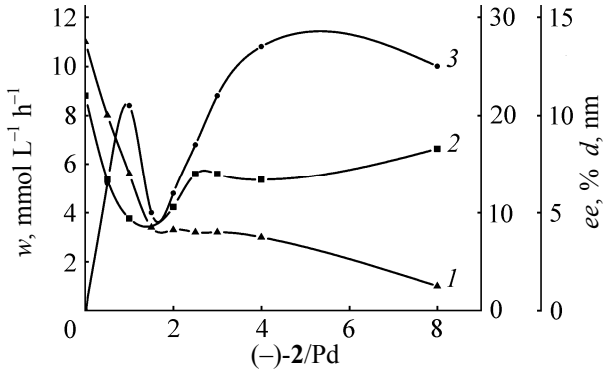

Fig. 2. Rate of acetophenone hydrogenation (*1*), excess of (*S*)-1-phenylethanol (*2*), and average size of nanoparticles (*3*) as functions of the (–)-**2**–Pd ratio in the $Pd(acac)_2$–*n*(–)-**2**–H_2 system.

The choice of the solvent also significantly affected the rate and enantioselectivity of the reaction. The plot of the rate and *ee* of the reaction as functions of ε_T did not reveal distinct correlation between the solvent polarity and *ee* (Fig. 3). Yet, dichloromethane was the best solvent in terms of both high rate and high enantioselectivity of the reaction. In the alcohols, the enantioselectivity was low, probably due to high solubility of the modifier resulting in the shift of the (–)-$\mathbf{2}_{solution}$ ↔ (–)-$\mathbf{2}_{surface}$ to left, and the decrease in the number of chiral-modified regions at the nanoparticles surface. It is interesting to notice that the substrate molecules could interact with alcohols via hydrogen bonding. The effect of alcohols on the reaction enantioselectivity (sometimes as prominent that the selectivity is reversed) has been found for the reduction of perfluorinated ketones on Pt/Al_2O_3 modified with (–)-**2** [35].

During the reaction, colloidal nanoparticles could aggregate and therefore lose the activity. Ammonium salts are usual electrostatic stabilizers, whereas polymers act as steric stabilizers [36]. In this study, we used the additional stabilizers to prevent the nanoparticles aggregation: cetyltrimethylammonium chloride (CTAC) and crosslinked poly-*N*-vinylpyrrolidone (CL-PVP). Despite slight increase in the activity of the system with CL-PVP, the *ee* for (*S*)-1-phenylethanol remained almost constant (Table 2).

When using $Pd(dba)_2$, common source of Pd(0), we observed high excess of the *S*-enantiomer product of the reaction (45.4%). The attempt to stabilize the

Table 1. Enantioselective hydrogenation of acetophenone in the presence of the $Pd(acac)_2$–(–)-**2**–H_2 system[a]

Exp. no.	Modifier/Pd	Conversion, %	w_{max}, mmol L^{-1} h^{-1}	Activity of catalyst, mol Sub/(mol Pd h)	*ee* (*S*), %
1	0	15	11±1	3.3±0.4	0
2	0.5	38	8.0±0.8	2.1±0.3	13±1.3
3	1	44	5.6±0.5	1.7±0.2	21±1.9
4	1.5	20	3.4±0.5	1.1±0.2	10±1.1
5	2	16	3.3±0.4	1.0±0.2	12±1.2
6	2.5	13	3.2±0.4	1.1±0.2	16±1.7
7	3	14	3.2±0.4	0.9±0.2	22±2.3
8	4	14	3.0±0.4	0.6±0.2	28±3.0
9	8	9	1.0±0.2	0.2±0.1	17±1.8

[a] c_{Pd} = 3.3 mmol/L, experiment duration 24–25 h, methanol as solvent.

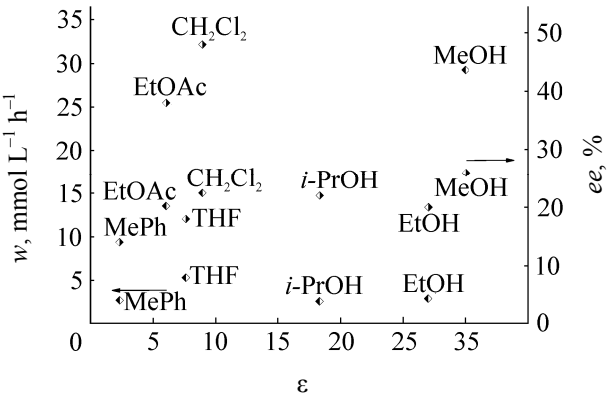

Fig. 3. Rate of hydrogenation and enantioselectivity of the reaction in the presence of the $Pd(acac)_2$–(–)-**2**–H_2 system as functions of dielectric constant of the solvent ε.

surface by addition of the polymer carrier CL-PVP resulted in the increase in w_{max} at complete conversion of the substrate, but enantioselectivity was significantly reduced (Table 2, Exp. 4 and 5). Likely, the palladium nanoparticles modified with (–)-cinchonidine were less involved in acetophenone hydrogenation due to the restrictions by the polymer network. Complete lifetime of the $Pd(dba)_2$–(–)-**2**–CL-PVP catalyst was 5 days at turnover number 400 mol/mol Pd (Table 2, Exp. 5).

The experiments with palladium on solid carrier Pd/C (Fig. 4) revealed that the rate of ketone hydrogenation was decreased by 10 times in the presence of (–)-cinchonidine. Low selectivity of the reaction with respect to the products typical of Pd/C (Fig. 4a) was retained 1-phenylethanol was reduced to ethylbenzene which resulted in the loss of the chiral product in the case of enantioselective process (Table 2, Exp. 6 and 7).

In the presence of the $Pd(acac)_2$–(–)-**2**–H_2 system, esters of ketoacids (methyl pyruvate and ethyl benzoylformate) were hydrogenated as well (Table 3). The rate of methyl pyruvate hydrogenation was slightly different from that of the reaction with acetophenone, but *ee* 54–56% for methyl ester of (*R*)-(–)-lactic acid at (–)-**2**/Pd ratio 1.5–2. Moreover, monitoring of *ee* during the reaction showed that it was decreasing from initial 85.6% to 56.0% at the end of the reaction. Enantioselectivity of the reaction of ethyl ester of (*S*)-(+)-mandelic acid formation from ethyl benzoylformate at the (–)-**2**/Pd ratio 2 : 1 was as low as 10%, the reaction rate being sufficiently high, 152.0 mmol L^{-1} h^{-1}. That was in good agreement with the data on high rate of hydrogenation of ethyl benzoylformate on Pd/Al_2O_3–(–)-**2** [21].

Study of the catalyst nature by physical methods. As often discussed in the literature [1, 37], the size of nanoparticles is a key factor determining the catalytic activity of palladium colloids. Palladium nanoparticles synthesized in the $Pd(acac)_2$–(–)-**2**–H_2 system at the (–)-**2**/Pd ratio of 0 to 8, were different in size (the high-resolution TEM data); the difference was sometimes huge. It should be noted that the introduction of cinchonidine improved the dispersity of the formed palladium nanoparticles: average nanoparticles size in the system where palladium black was formed was of 10 nm, being of 4.8 nm in the $Pd(acac)_2$–(–)-**2**–H_2 system.

Table 2. Reaction rate and the catalyst activity depending on the nature of palladium precursor and stabilizer[a]

Exp. no.	System	Conversion, %	w_{max}, mmol L^{-1} h^{-1}	Activity of catalyst, mol Sub/(mol Pd h)	*ee* (*S*), %
1	$Pd(acac)_2$–(–)-**2**	44.2	5.6±0.5	1.7±0.2	21.0±2.0
2	$Pd(acac)_2$–CTAC–(–)-**2**	72.4	6.3	1.9	23.2±2.0
3	$Pd(acac)_2$–(–)-**2**–CL PVP	27.4	17.6	5.1	24.3±2.0
4	$Pd(dba)_2$–(–)-**2**	38.5	13.8	4.1	45.4±3.4
5	$Pd(dba)_2$–(–)-**2**–CL PVP (portion 1)	100	42±5.1	12.6±1.5	18.2±2.0
	(portion 2)	100	88.5±8.6	26.6±2.5	17.8±2.0
	(portion 3)	100	42.1±8.6	12.7±2.0	18.2±2.0
6	Pd/C	100	300±15	91±5	0
7	Pd/C–(–)-**2**	100	35.4	10.6	25.6±2.0

[a] c_{Pd} = 3.3 mmol/L, experiment duration 24–25 h, toluene–methanol, 3 : 20.

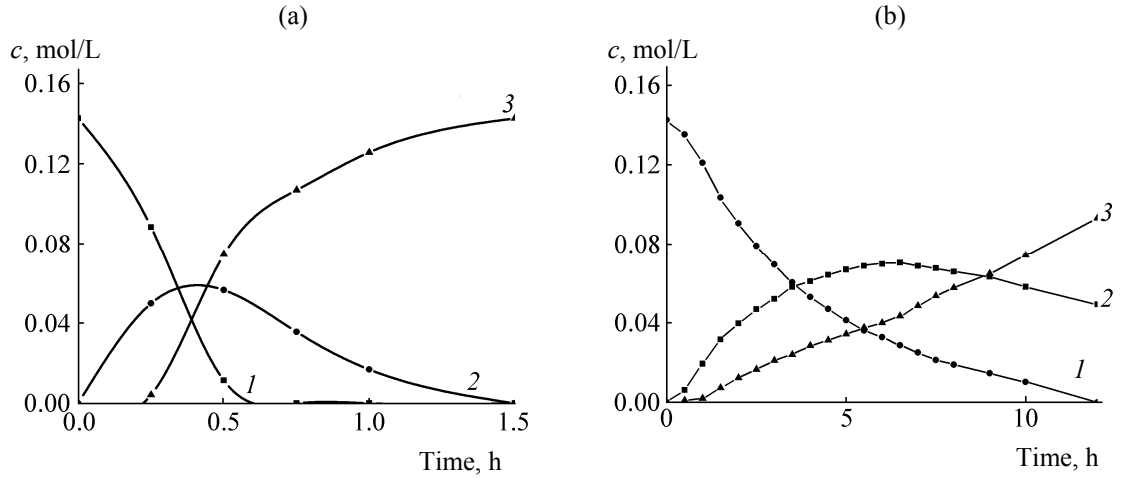

Fig. 4. Kinetic curves of acetophenone hydrogenation on Pd/C in the absence (a) and in the presence of the modifier (b) at (–)-**2** : Pd = 1: (*1*) acetophenone, (*2*) 1-phenylethanol, and (*3*) ethylbenzene.

The electron microscopy images of the colloidal dispersions contained the high-contrast nanoparticles, predominantly spherical. The atoms lattice observed in high-resolution TEM images evidenced high crystallinity of the formed nanoparticles. The measured interlayer spacings (2.2417, 1.9388, 1.3723, and 1.1749 Å) corresponded to crystallographic planes of palladium: 111 (2.2458 Å), 200 (1.9451 Å), 220 (1.3754 Å), and 311 (1.173 Å) (PDF-2, no. 00-046-1043). According to the electron diffraction data, the particles were polycrystalline and arranged in different crystallographic directions.

Histograms of distribution of nanoparticles in the $Pd(acac)_2$–(–)–**2**–H_2 system for the (–)-**2**/Pd ratios 0.5, 1, and 8 obtained by statistical analysis of 200–250 nanoparticles are shown in Fig. 5. Energy-dispersive X-ray microanalysis of various parts of the sample at n = 1 evidenced the sample heterogeneity and the presence of palladium and carbon in it. At the same time, the C/Pd ratio could not be determined, because carbon was deposited onto copper grid for TEM. The elements ratio was determined by means of TGA.

Thermograms of Pd sample isolated from the $Pd(acac)_2$–(–)-**2**–H_2 system (Fig. 6) contained the regions corresponding to evaporation of residual solvent (87–126°C) as well as melting (165–245°C) and decomposition of (250–700°C) (–)-cinchonidine. The final mass loss of the sample was 62.8%, and the sample composition was estimated as $Cin_{0.6}Pd$. According to the reference data [38], heating at above 300–350°C resulted in the formation of thin PdO film at the palladium surface, which was decomposed into the metal and oxygen above 850°C. Probably, the slight mass loss above 1010°C was due to decomposition of palladium oxide. Formation of palladium nitrides and carbides is possible only at high temperature and pressure [39], moreover, no additional reflections were observed in the X-ray diffraction patterns. The X-ray

Table 3. Hydrogenation of methyl pyruvate and ethylbenzoyl formate in the presence of the $Pd(acac)_2$–(–)-**2**–H_2 system[a]

Exp. no.	(–)-**2** : Pd	Substrate	Conversion, %	w, mmol L^{-1} h^{-1}	Activity of catalyst, mol Sub/(mol Pd h)	*ee*, %
1	1.0	Methyl pyruvate	30	8.5±1.1	2.6±0.3	23.4±2.6 (*R*)
2	1.0	Ethyl benzoylformate	71	152.0±13.8	45.2±5.1	2.2±0.3 (*S*)
3	1.5	Methyl pyruvate	12	1.6±0.2	0.5±0.1	54.3±6.6 (*R*)
4	2.0	Methyl pyruvate	13	1.2±0.1	0.4±0.1	56.0±6.8 (*R*) 85.6 (*R*)
5	2.0	Ethyl benzoylformate	58	133.7±12.5	40±1.1	10.2±1.6 (*S*)

[a] c_{Pd} = 3.3 mmol/L, experiment duration 24–25 h, toluene–methanol, 3 : 20.

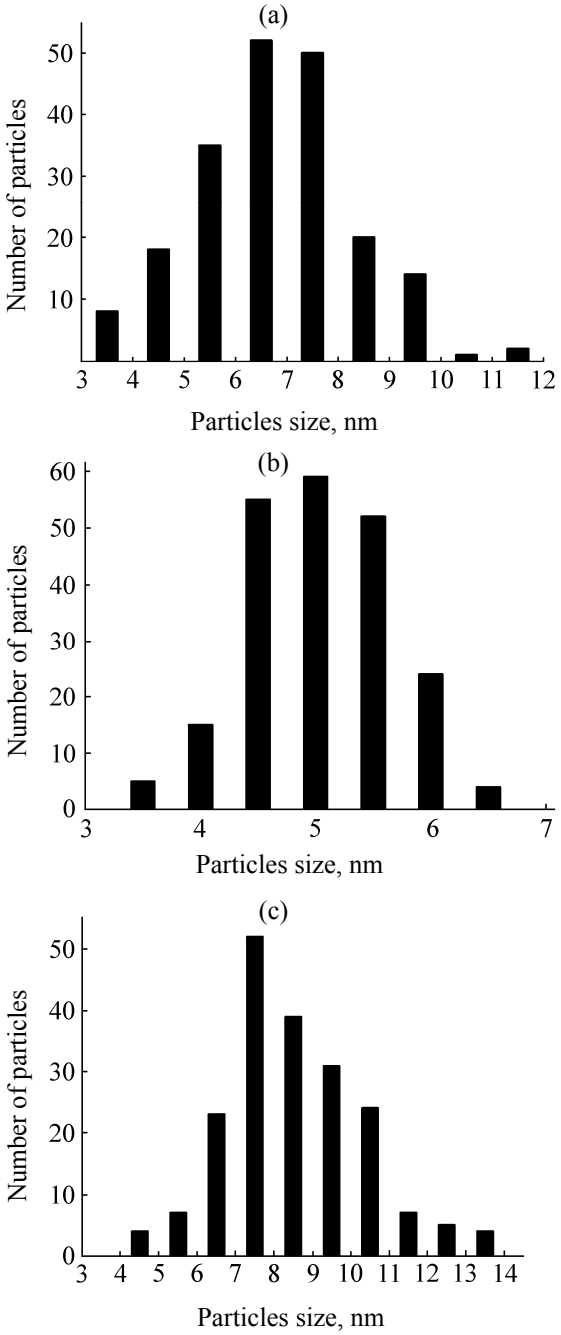

Fig. 5. Histograms of the nanoparticles distribution in the $Pd(acac)_2$–*n*(–)-**2**–H_2 system at *n* = 0.5 (a, weighted-mean size 6.7 nm, σ 1.6 nm), 1 (b, weighted-mean size 4.7 nm, σ 0.6 nm), 8 (c, weighted-mean size 8.3 nm, σ 2.0 nm).

diffraction pattern of solid dispersed phase isolated from the $Pd(acac)_2$–(–)-**2**–H_2 system contained broadened diffraction maximums at 2θ 35°–80° assigned to the reflections from crystallographic planes (111), (200), and (220) of face-centered cubic Pd lattice *Fm*3*m* (40.1°, 46.6°, and 68.1°, respectively,

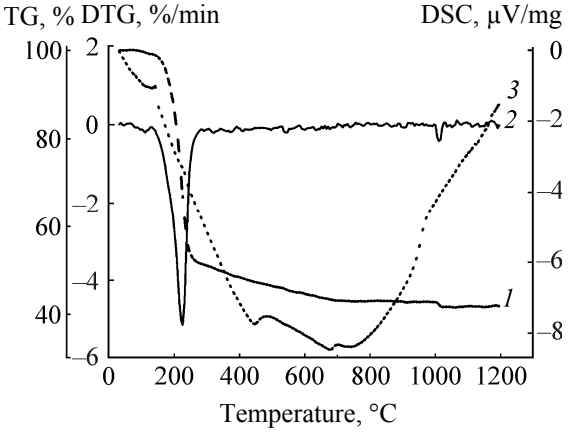

Fig. 6. Thermogram of the sample isolated from the $Pd(acac)_2$–(–)-**2**–H_2 system.

according to PDF-2, no. 00-046-1043). The coherent scattering area size calculated from the half-width of the (111) line using the Scherrer equation gave 4.8 nm, in line with the average size determined from TEM data.

Analysis of histograms of size distribution of the nanoparticles in the $Pd(acac)_2$–*n*(–)-**2**–H_2 systems revealed that the increase in the (–)-**2**/Pd ratio from 0.5 to 1 led to the decrease in the average particles size from 6.7±1.6 to 4.7±0.6 nm (Fig. 5). At the same time, the changes in the particles size in the $Pd(acac)_2$–*n*(–)-**2**–H_2 system and the rate of acetophenone hydrogenation were coinciding (Fig. 2) over the (–)-**2**/Pd molar ratio 0–1. Up to (–)-**2**/Pd = 1, cinchonidine served as efficient stabilizer preventing the nanoparticles growth, and at the (–)-**2**/Pd ratio from 2 to 3.5 the reaction rate grew with the increase in the average size of Pd nanoparticles.

TEM images analysis revealed that anisotropic particles (10–18%) were formed over the mentioned ratio range, whereas at (–)-**2**/Pd below 2 and above 3.5 exclusively spherical particles were formed. The appearance of non-spherical particles led to the increase in the specific area of the active nanoparticles surface, explaining the reaction acceleration over that range of molar ratio.

Deviation of the nanoparticles shape from spherical could be due to the change in the type of chemisorption of (–)-cinchonidine at the metal surface. Enantioselectivity is governed by the molecular orientation of (–)-cinchonidine at chiral catalytic interface nanoparticle–liquid. Adsorbed (–)-cinchonidine can take three types of orientation with respect to

Pt surface: planar, with the plane of quinoline ring forming strong π-bonding with surface metal atom (F1), and two lateral ones [40, 41]. In one of the lateral orientations the molecule forms the α-C–Pt bond with the metal (the aromatic hydrogen atom being eliminated) and a donor bond via the electron pair of nitrogen (T2), the other lateral orientation is characterized by only weak bonding via nitrogen (T3).

To get the information on the coating of the surface at the (–)-**2**/Pd ratio = 1, critical in view of enantioselective properties of the system, we recorded the IR spectra of crystalline (–)-cinchonidine, its solution in $CHCl_3$, and the $Pd(acac)_2$–*n*(–)-**2**–H_2 system in $CHCl_3$. Analysis of the spectra revealed that the F1 (1175, 1383, 1439, and 1560 cm^{-1}) and T2 (1212, 1383, 1439, and 1560 cm^{-1}) orientation types prevail at palladium surface at (–)-**2**/Pd =1. Probably, the increase in the (–)-**2**/Pd ratio led to the decrease in the fraction of strongly bound adsorbed (–)-cinchonidinea, and the weakly bound modifier molecules were readily replaced by the substrate molecules, thus enhancing the contribution of the non-modified surface in the catalysis. At even higher concentration of the modifier, the weakly bound forms could be substituted with the π-coordinated one, thus resulting in the growth in the enantioselectivity.

In summary, the rate and enantioselectivity of hydrogenation of acetophenone and esters of pyruvic and benzoylformic acids on palladium nanoparticles modified with natural (–)-cinchonidine are complex functions of the (–)-**2**/Pd ratio, nature of the solvent, the palladium precursor, and substrate, as well as the presence of a carrier. To optimize the system, soft carriers (polymers) should be used to increase the catalyst lifetime in combination with nanoparticles with narrow size distribution.

EXPERIMENTAL

Acetophenone (Acros Organics, 99%), methyl pyruvate, methyl benzoylformate (Aldrich, 95%), and the solvents (methanol, propanol-2, toluene, dichloromethane, and hexane) were thoroughly dried, distilled, and stored under argon. $Pd(acac)_2$ was synthesized as described elsewhere [42]; from $Pd(dba)_2$ (Acros Organics) used as received.

High-resolution transmission electron microscopy (TEM) images were obtained using a FEI Tecnai G^2 device (accelerating voltage 200 kV) equipped with an energy-dispersive analyzer (EDX) to perform elemental analysis; resolution of 0.19 nm was reached. A drop of a solution of the *in situ* formed catalyst (c_{Pd} 1–5 mol/L) was applied on a carbon-coated copper grid and dried in argon. The images parameters and particles morphology and microstructure were determined using iTEM 5.0 and Digital Micrograph 2.30 software. To analyze the periodic structures and filter the images, FFT and iFFT Fourier methods were used. Nanoparticles size distribution was determined by measuring the size of 200–250 Pd nanoparticles in several TEM images taken from different parts of the grid.

X-ray diffraction analysis was performed using a Shimadzu XRD 7000 diffractometer with copper anode, $\lambda(K_\alpha)$ 0.15418 nm. The focusing was performed using a Bragg–Brentano scheme with a monochromator at the diffracted beam (angles range 3.000°–80.000°, scan step 0.05°). The phases were identified using Match! 1.1 software and PDF-2 database. Average size of palladium crystallites was determined from half-width of the (111) in 2θ scale using the Scherrer equation.

IR spectra were recorded using a 3100 FT IR spectrometer (Varian) over 1100–5000 cm^{-1} (solution in chloroform, CaF_2 cell, layer thickness 0.1 mm). Thermal analysis (TG, DTG, and DSC) was performed using a NETZSCH STA 449F3 instrument (25–1000°C, heating rate 10 deg/min, argon stream 20 mL/min). The samples for XRD and TGA were isolated from the catalytic systems, washed with isopropanol, dried at reduced pressure at 50°C, and stored under argon in sealed ampoules.

Specific rotation of the pure compounds was determined using an ADP410 automated digital polarimeter at wavelength 589 nm (optical pathlength 50 mm, concentrations of the solutions 2–30 g/100 mL of solvent). Analysis of the hydrogenation products was performed using a Shimadzu GCMS-QP2010 Plus chromato–mass spectrometer (EI 70 eV, scan over *m*/*z* 40–350, capillary column Equity 5 (30 m × 0.25 mm, 95% dimethylpolysiloxane + 5% diphenylpolysiloxane, helium as carrier gas). Enantiomer excess (*ee*, %) was determined using a GC Agient 7890A gas chromatograph equipped with a Dina switch, flame ionization detector, a CYCLODEX-B chiral capillary column (30 m × 0.25 mm), and a 5% Phenyl Methyl Siloxane capillary column (30 m × 0.25 mm). Temperature program: heating from 70 to 160°C at

3 deg/min, gas flow rate 1.5 mL/min, thermostat temperature 115°C.

Hydrogenation procedure. Hydrogenation reaction was performed in a Picoclave GlassUster cyclone 075 BUCHI autoclave. A solution of the precursor and the modifier: 0.0304 g (1×10^{-4} mol) of palladium acetylacetonate, ~10^{-4} mol of the modifier, 3 mL of toluene, and 19 mL of methanol was transferred to a 100 mL vessel being bubbled with hydrogen. The pale-yellow solution was stirred under hydrogen pressure of 5 atm during 30 min, then 0.5 mL of the substrate in 8 mL of methanol was added, and the "zero sample" was withdrawn. The mixture of hydrogenation products was then analyzed each 30 or 60 min using the chromato–mass spectrometer. Configuration of the prevailing enantiomer was determined by comparison with the reference data [43].

REFERENCES

1. Bukhtiyarov, V.I. and Slin'ko, M.G., *Russ. Chem. Rev.*, 2001, vol. 70, no. 2, p. 147. doi 10.1070/RC2001v070n02ABEH000637
2. Borah, B.J., Saikia, K., Saikia, P.P., Barua, N.Ch., and Dutta, D.K., *Catalysis Today*, 2012, vol. 198, no. 1, p. 174. doi 10.1016/j.cattod.2012.03.083
3. Dinç, M., Metina Ö., and Özkar, S., *Catalysis Today*, 2012, vol. 183, no. 1, p. 10. doi 10.1016/j.cattod.2011.05.007
4. Zhu, C., Zeng, J., Lu, P., Liu, J., Gu, Zh., and Xia, Y., *Chem. Eur. J.*, 2013, vol. 19, no. 16, p. 5127. doi 10.1002/chem.201203787
5. Zhang, H., Jin, M., Xiong, Y., Lim, B., and Xia, Y., *Acc. Chem. Res.*, 2013, vol. 46, no. 8, p. 1783. doi 10.1021/ar300209w
6. Ramsurn, H and, Gupta, R.B., in *New and Future Developments in Catalysis. Catalysis by Nanoparticles*, Suib, S.L., Ed., Amsterdam; Boston; Heidelberg: Elsevier, 2013, ch. 15, p. 347.
7. Mallick, K., Witcomb, M., J., Dinsmore, A., and Scurrell, M.S., *J. Mater. Sci.*, 2006, vol. 41, no. 6, p. 1733. doi 10.1007/s10853-006-3950-7
8. Pushkarev, V.V., Zhu, Z., An, K., Hervier, A., and Somorjai, G.A., *Top Catal.*, 2012, vol. 55, nos. 19–20, p. 1257. doi 10.1007/s11244-012-9915-y
9. Roy, S. and Perics, M.A., *Org. Biomol. Chem.*, 2009, vol. 7, no. 13, p. 2669. doi 10.1039/b903921j
10. Barbaro, P., Santo, V.D., and Liguori, F., *Dalton Trans.*, 2010, vol. 39, no. 36, p. 8391. doi 10.1039/c002051f
11. Harris, K.D.M. and Thomas, J.M., *ChemCatChem.*, 2009, vol. 1, no. 2, p. 223. doi 10.1002/cctc.200900181
12. Wu, B. and Zheng, N., *Nano Today*, 2013, vol. 8, no. 2, p. 168. doi 10.1016/j.nantod.2013.02.006
13. Watt, J., Cheong, S., and Tilley, R.D., *Nano Today*, 2013, vol. 8, no. 2, p. 198. doi 10.1016/j.nantod.2013.03.001
14. Semagina, N., Renken, A., and Kiwi-Minsker, L., *J. Phys. Chem. (C)*, 2007, vol. 111, no. 37, p. 13933. doi 10.1021/jp073944k
15. Semagina, N., Renken, A., Laub, D., and Kiwi-Minsker, L., *J. Catalysis*, 2007, vol. 246, no. 2, p. 308. doi 10.1016/j.jcat.2006.12.011
16. Yasukawa, T., Miyamura, H., and Kobayashi, S., *ACS Catal.*, 2016, vol. 6, no. 11, p. 7979. doi 10.1021/acscatal.6b02446
17. Yasukawa, T., Suzuki, A., Miyamura, H., Nishino, K., and Kobayashi, S., *J. Am. Chem. Soc.*, 2015, vol. 137, no. 20, p. 6616. doi 10.1021/jacs.5b02213
18. Bartók, M., Felföldi, K., Szöllösi, G., and Bartók, T., *Catal. Lett.*, 1999, vol. 61, no. 1, p. 1. doi 10.1023/A:1019008519015
19. Baiker, A., *J. Mol. Cat. (A)*, 2000, vol. 163, nos. 1–2, p. 205. doi 10.1023/A:1019008519015
20. Murzin, D.Yu. and Toukoniitty, E., *React. Kinet. Catal. Lett.*, 2007, vol. 90, no. 1, p. 19. doi 10.1007/s11144-007-5004-9
21. Szöllösi, G., Hermán, B., Fülöp, F., and Bartók, M., *React. Kinet. Catal. Lett.*, 2006, vol. 88, no. 2, p. 391. doi 10.1007/s11144-006-0076-5
22. Burgi, T. and Baiker, A., *Acc. Chem. Res.*, 2004, vol. 37, no. 11, p. 909. doi 10.1021/ar040072l.
23. Margitfalvi, J.L. and Tfirst, E., *J. Mol. Cat. (A)*, 1999, vol. 139, no. 1, p. 81. doi 10.1016/S1381-1169(98)00197-6
24. Bartók, M., Balázsik, K., and Notheisz, F., *React. Kinet. Catal. Lett.*, 2002, vol. 77, no. 2, p. 363. doi 10.1023/A:1020852405963
25. Yasukawa, T., Suzuki, A., Miyamura, H., Nishino, K., and Kobayashi, S., *J. Am. Chem. Soc.*, 2015, vol. 137, no. 20, p. 6616. doi 10.1021/jacs.5b02213
26. Bonnemann, H. and Braun, G.A., *Chem. Eur. J.*, 1997, vol. 3, no. 8, p. 1200. doi 10.1002/chem.19970030805
27. Studer, M., Blaser, H.-U., and Exner, C., *Adv. Synth. Catal.*, 2003, vol. 345, no. 1–2, p. 45. doi 10.1002/adsc.200390029
28. Mink, L., Ma Zh., Olsen, R.A., James, J.N., Sholl, D.S., Mueller, L.J., and Zaera, F., *Top Catal.*, 2008, vol. 48, nos. 1–4, p. 120. doi 10.1007/s11244-008-9041-z
29. Hisaki, I., Hiraishi, E., Sasaki, T., Orita, H., Tsuzuki, S., Tohnai, N., and Miyata, M., *Chem. Asian J.*, 2012, vol. 7, no. 11, p. 2607. doi 10.1002/asia.201200566
30. Kubota, J. and Zaera, F., *J. Am. Chem. Soc.*, 2001, vol. 123, no. 44, p. 11115. doi 10.1021/ja016722n

31. Mallat, T., Orglmeister, E., and Baiker, A., *Chem. Rev*., 2007, vol. 107, no. 11, p. 4863. doi 10.1021/cr0683663
32. Huang, Y., Chen, J., Chen, H., Li, R., Li, Y., Min, L., and Li, X., *J. Mol. Cat. (A)*, 2001, vol. 170, nos. 1–2, p. 143. doi 10.1016/S1381-1169(01)00053-X
33. Collier, P.J., Hall, T.J., Iggo, J.A., Johnston, P., Slipszenko, J.A., Wells, P.B., and Whyman, R., *Chem. Commun*., 1998, no. 14, p. 1451. doi 10.1039/A803901A
34. Zhang, J., Yan, X., and Liu, H., *J. Mol. Cat. (A)*, 2001, vol. 176, nos. 1–2, p. 281. doi 10.1016/S1381-1169(01)00268-0
35. Vargas, A., Hoxha, F., Bonalumi, N., Mallat, T., and Baiker, A., *J. Catal*., 2006, vol. 240, no. 2, p. 203. doi 10.1016/j.jcat.2006.03.022
36. Gniewek, A., Ziółkowski, J.J., Trzeciak, A.M., and Kępiński, L., *J. Catal*., 2006, vol. 239, no. 2, p. 272. doi 10.1016/j.jcat.2006.02.002
37. Durand, J., Teuma, E., and Gómez, M., *Eur. J. Inorg. Chem*., 2008, p. 3577. doi 10.1002/ejic.200800569
38. *Khimicheskaya entsiklopediya* (Chemical Encyclopedia), Knunyants, I.L., Ed., Moscow: Bol'shaya Rossiiskaya Entsiklopediya, 1992, vol. 3, p. 440.
39. Ivanovskii, A.L., *Russ. Chem. Rev*., 2009, vol. 78, no. 4, p. 303. doi 10.1070/RC2009v078n04ABEH004036
40. Baiker, A., *Catalysis Today*, 2005, vol. 100, p. 159. doi 10.1016/j.cattod.2004.12.001
41. Kraynov, A., Suchopar, A., and Richards, R., *Catal. Lett*., 2006, vol. 110, nos. 1–2, p. 91. doi 10.1007/s10562-006-0090-2
42. USA Patent 3474464, 1969; *Ross. Zh. Khim.*, 1970, 19N102P.
43. Chambers, W.J., Brasen, W.R., and Hause Ch.R., *J. Am. Chem. Soc*., 1957, vol. 79, no. 4, p. 879. doi 10.1021/ja01561a025